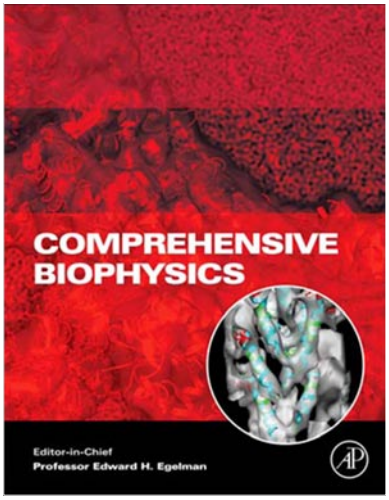

From S. Mondal, H. Weinstein and G. Khelashvili, Interactions of the Cell Membrane with Integral Proteins. In: Edward H. Egelman, editor: Comprehensive Biophysics, Vol 9, Simulation and Modeling, Harel Weinstein. Oxford: Academic Press, 2012. pp. 229-242.
ISBN: 978-0-12-374920-8

9.12 Interactions of the Cell Membrane with Integral Proteins

S Mondal, H Weinstein, and G Khelashvili, Weill Cornell Medical College of Cornell University, New York, NY, USA

Abbreviations

5HT	5-hydroxytryptamine (serotoVolume 9nin)
DHA	Docosahexaenoic acid
DLPC	1,2-dilauroyl-*sn*-glycero-3-phosphocholine
DMPC	1,2-dimyristoyl-*sn*-glycero-3-phosphocholine
DOPC	1,2-dioleoyl-*sn*-glycero-3-phosphocholine
DOPE	1,2-dioleoyl-*sn*-glycero-3-phosphoethanolamine
DynA	DynorphinA
EPR	electron paramagnetic resonance
FRET	forster resonance energy transfer
GPCR	G-protein coupled receptor
KET	ketanserin
KOR	kappa-opioid receptor
LSD	lysergic acid diethylamide
MD	molecular dynamics
NMR	nuclear magnetic resonance
PC	phosphatidylcholine
PE	phosphatidylethanolamine
POPC	1-palmitoyl-2-oleoyl-*sn*-glycero-3-phosphocholine
SASA	solvent accessible surface area
SDPC	1-stearoyl-2-docosahexaenoyl-*sn*-glycero-3-phosphocholine
TM	transmembrane segment

Glossary

Atomic force microscopy A high-resolution experimental technique that probes the surface of specimens using a cantilever system, and can be applied to map out protein structure at the level of single molecules.

Channel open probability The probability of the channel being in the open state, a key observable for ion channels in patch clamp experiments.

Electron paramagnetic resonance An experimental spectroscopic technique that allows observation of specific quantum mechanical magnetic properties of chemical species with unpaired electrons, and can be applied to study lipid association of membrane proteins.

Förster resonance energy transfer A mechanism describing non-radiative energy transfer between two chromophores.

G-protein coupled receptor Seven-transmembrane domain receptors that sense molecules outside the cell and activate inside signal transduction pathways and, ultimately, cellular responses.

Hydrophobic mismatch The difference between the hydrophobic thickness of a transmembrane segment and the bulk hydrophobic thickness of the lipid bilayer.
Molecular dynamics A computational method that solves Newtonian mechanics to simulate the dynamics of an N-body system, and may be applied to simulate the dynamics of membrane-protein systems at the atomistic level.
Nuclear magnetic resonance An experimental spectroscopic technique that allows the observation of specific quantum mechanical magnetic properties of atomic nuclei with non-zero spin, which can be applied to study the transfer of magnetization within the protein and between the protein and the first shell of lipids.
Residual mismatch The hydrophobic mismatch between the hydrophobic thickness of a transmembrane segment and that of the adjacent deformed lipid bilayer. The residual mismatch occurs if the hydrophobic mismatch at a transmembrane segment is not alleviated by the membrane deformation.
Solvent accessible surface area The surface area of a residue that is exposed to the solvent.

For a long time, the cell membrane was considered to be no more than a passive structure that compartmentalized the cell. However, this perception has been challenged by increasing evidence that the lipid environment modulates the function and organization of the membrane proteins.[1,2] This evidence comes from a range of biophysical and biochemical experiments, encompassing spectroscopic, imaging, patch clamp and other techniques.[3–7] Many observations of the effect of the lipid membrane on protein function have been largely explained in terms of the energy cost due to hydrophobic mismatch between the membrane and the protein.[2,8] The purpose of this chapter is to present a computational framework for quantifying hydrophobic mismatch-induced membrane remodeling and corresponding energetics, along with illustrative applications of the methodology to specific membrane-protein systems.

9.12.1 Evidence for Role of Lipid Environment for Membrane Protein Function

We begin by presenting some of the findings regarding the role of the lipid membrane in membrane protein function, largely focusing on the specific biological systems and findings that we believe will help the reader to better establish the biological context of the illustrative applications discussed in section 9.12.4.

9.12.1.1 Lipid Environment and G-Protein Coupled Receptors (GPCRs) – Receptor Activation and Oligomerization

Overwhelming evidence indicates that the activity and organization of GPCR proteins are regulated at various spatial scales, and involve different membrane components. For example, experimental evidence suggests that many GPCRs function with different efficacy when localized in cholesterol-enriched lipid domains, or rafts.[9–11] Furthermore, ligands for certain GPCRs, such as cannabinoid and opioid receptors, are membrane soluble, e.g., the well-known AM841 ligand for cannabinoid CB-2 GPCR,[12,13] and Dynorphin A for the kappa-opioid receptor (KOR).[14,15] As these ligands have an ability to interact directly with cell membranes before they reach their host receptor,[12] the critical question is: how do membrane components and cholesterol modulate the interaction of such ligands with their host GPCRs? In Section 9.12.4, we apply the quantitative framework presented in this chapter to answer this question and provide mechanistic insights into the role of cholesterol in regulating function of KOR receptors.

An effect of the lipids on the equilibrium distribution between active and inactive GPCR conformations has also been reported. A particularly well-studied example is that of rhodopsin, which has long served as a prototypical Class-A GPCR for understanding GPCR structure and function in general. Rhodopsin accounts for $>90\%$ of the proteins in rod outer disk membranes and is responsible for dim light vision via the transduction of photons into an intracellular biochemical signal. The photochemical function of rhodopsin has been shown to be affected by key characteristics of lipids at the molecular level, viz., acyl chain length, unsaturation of the acyl chain, headgroup size, and headgroup charge[16–20] (**Figure 1**). Specifically, flash photolysis experiments, which measure the amount of rhodopsin in its inactive Metarhodopsin I and its active Metarhodopsin II conformations in response to a single flash of light, have shown that the equilibrium between the two conformations is sensitive to the lipid environment.

$$\text{Metarhodopsin I} + H_3O^+ \leftarrow \rightarrow \text{Metarhodopsin II}$$

Thus, in mixtures of 1,2-dioleoyl-*sn*-glycero-3-phosphocholine (DOPC) and 1,2-dioleoyl-*sn*-glycero-3-phosphoethanolamine (DOPE) lipids, there is an increase in Metarhodopsin II with increasing molar fraction of DOPE lipid.[20] The presence of PE headgroups shifts the equilibrium to the right relative to PC headgroups. A similar shift is observed on increasing the molar fraction of lipids containing the negatively charged PS headgroup[21] and the molar fraction of the highly unsaturated Docosahexaenoic acid (DHA)-containing lipids.[18]

It should be noted that such lipid-mediated modulation of rhodopsin function is not due to lipids of a specific chemical nature, as the basic molecular characteristics of lipids do not have mutually exclusive effects. For example, a lipid mixture of DOPE and DOPC in the molar ratio of 75:25 gives similar results compared to native ROS membranes (which contain a lower mole fraction of DOPE but contain lipids with PS headgroups and DHA-containing lipids).[20] Thus, lipids containing PE

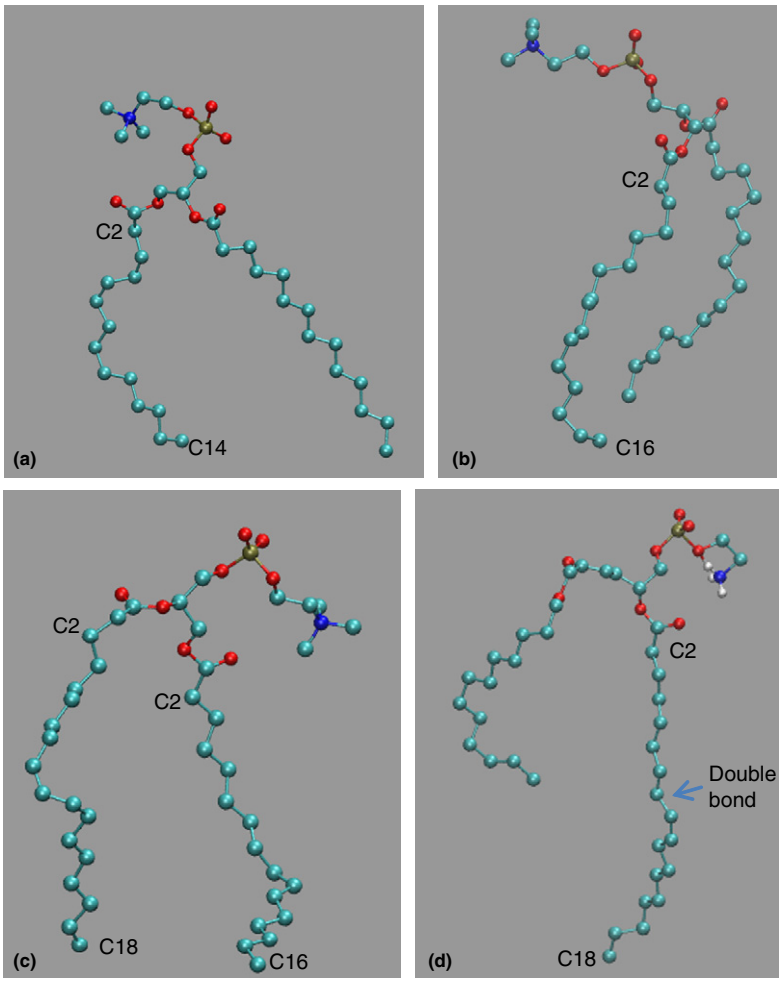

Figure 1 Schematic drawing of several common lipid molecules used in the model membrane systems discussed here, illustrating the structural characteristics at the molecular level. (a) DMPC, with two 14-carbon (C) long acyl chains, (b) DPPC, with two 16-C acyl chains, (c) POPC, containing a 16-C tail saturated acyl chain and a 18-C monounsaturated acyl chain, (d) POPE, similar to POPC but with PE rather than PC headgroup. The color scheme is: cyan: C, blue: N, gold: P, red: O, white: H. H atoms are shown only in the headgroups. The C2 atom and the last C atom of the acyl chain are labeled. For this figure, the configuration of each lipid was chosen randomly from a lipid membrane patch in the MD simulations.

headgroups can compensate for the absence of unsaturated lipids and negatively charged headgroups.

Current evidence for the involvement of the lipid membrane environment is not limited to Class A GPCRs. For example, the ligand binding for the Class C GPCR metabotropic glutamate receptor has been found to depend on the lipid composition, with a cholesterol-rich environment resulting in a higher affinity for glutamate.[22]

Another critical role that the lipid environment has been shown to play in relation to GPCR function is in the process of oligomerization of these receptors. GPCRs can function in monomeric form[23] and for many years this was considered to be its physiological level of organization. Yet several GPCRs have now been found to form dimers or higher-order oligomers[24] with consequences for function,[25–27] a topic that has naturally engaged the attention of the GPCR community of late. Of particular relevance to this chapter, the oligomerization of rhodopsin has been found to depend on the lipid membrane environment. Forster resonance energy transfer (FRET) data on rhodopsin reconstituted in monounsaturated lipid bilayers of different tail lengths showed that the extent of oligomerization is much lower for $(C20:1)_2PC$ than it is for $(C14:1)_2PC$.[28] Coarse-grained molecular dynamics (MD) simulations of these systems suggest that the oligomerization interface may also be different in $(C14:1)_2PC$ compared to $(C20:1)_2PC$.[29] In Section 9.12.4, using the quantitative framework described in this chapter, we shall examine membrane-driven GPCR oligomerization from an energetic standpoint leading to mechanistic insights.

Notably, the activation and oligomerization of GPCRs have been found to be related, and experimental studies show that agonist and inverse agonist stabilize different oligomerization interfaces for certain GPCRs such as the serotonin 5-HT_{2C}, dopamine D2, and beta-2 adrenergic GPCRs.[30–32] For example, cysteine-crosslinking experiments with dopamine D2 revealed that the face of TM4 involved in the dimerization interface is different when measured in the presence of the agonists dopamine or quinpirole vs. the inverse agonist sulpiride.[32] The

quantitative framework we present here is used to examine a possible role of the lipid environment in the ligand-induced oligomerization of GPCRs (Section 9.12.4).

9.12.1.2 Role of Lipid Environment in Ion Channel Function

The functioning of ion channels has also been shown to be affected by the membrane environment. The lipid bilayer plays a central role in the gating of mechanosensitive channels, with the open probability being dependent on the membrane tension.[2] Changes in the bilayer properties, therefore, affect the open probability of these channels.

The functioning of ion channels that are not gated by the membrane tension as part of their physiological mechanism has also been found to depend on the lipid membrane environment. One of the most well-studied examples is that of gramicidin channels,[8] which are cation-selective channels formed by the transbilayer association of two 15-amino acid beta helical units in a reversible process. The lifetime and appearance frequency of these channels (but not their single channel conductance) have been found to be sensitive to the lipid bilayer thickness and material properties, and this dependency could be quantitatively explained using tools based on concepts of lipid-protein interactions (described in later sections of this chapter).[33,34] In fact, these channels have come to be used as molecular probes to measure the effect of pharmacological interventions on bilayer properties.[8]

Modifiers of bilayer properties have been shown to affect the function of various ion channels without chemically specific interactions with the channel.[35] For example, physiologically relevant concentrations of capsaicin increase the lifetime of gramicidin channels, with a similar concentration dependence for both left-handed and right-handed gramicidin channels, and this effect is inferred to be a result of a decrease in the bilayer stiffness.[5] Whole cell patch clamp recordings show that capsaicin also promotes the deactivation of voltage-dependent sodium channels and N-type calcium channels via a hyperpolarizing shift in the inactivation potential.[5] Similar effects have been observed for a number of structurally different bilayer modifiers, each of which has been found to affect several different ion channels without direct chemical interactions[36–38] (for a summary, please see Table 4 of ref. 8).

9.12.2 Key Elements of Lipid-Protein Interactions

The effect of the lipid membrane on the protein function can be exerted through interactions between the lipid and the protein at specific sites, as well as through deformation of the lipid membrane.

Among the first lines of evidence that membrane components, such as cholesterol, can directly interact with GPCRs at specific locations around the receptor, came from experimental structural studies[39–41] on beta2 adrenergic receptors and rhodopsin, where the receptors were co-crystallized with cholesterol molecules at specific sites around the GPCRs. Molecular dynamics simulations also predicted that certain regions on the rhodopsin molecule were engaged in direct interactions with cholesterol at microsecond time-scales.[42,43] Furthermore, the longer time-scale dynamics of cholesterol at these specific binding sites were found to be related to conformational changes in rhodopsin associated with the receptor activation.

MD simulations and solid-state nuclear magnetic resonance (NMR) experiments also revealed the existence of site-specific interactions of rhodopsin with polyunsaturated DHA-containing lipids.[4,44] Such interactions can interfere with interhelical contacts, more so in certain conformations of the protein. In this way, these interactions can stabilize certain conformations relative to others.

In addition to specific interactions between membrane components and GPCRs, the material properties of the lipid membranes have also been shown to affect protein function. Such a non-specific mode of interaction has been suggested as a possible mechanism in regulating rhodopsin activation and oligomerization,[3,28] and the lifetime of active gramicidin channels in different lipids.[33,34] These non-specific effects have been explained in terms of the energy cost of membrane deformations caused by "hydrophobic mismatch", defined as the difference between the hydrophobic thickness of the unperturbed membrane and that of the protein. In the presence of such a hydrophobic mismatch, the membrane deforms in order to alleviate the energy cost of the mismatched interface. For example, X-ray diffraction measurements of the phosphate-to-phosphate distances of 1,2-dimyristoyl-*sn*-glycero-3-phosphocholine (DMPC) and 1,2-dilauroyl-*sn*-glycero-3-phosphocholine (DLPC) bilayers with and without gramicidin channels showed that the thinner DLPC membrane and the thicker DMPC membrane deformed towards a common intermediate value when gramicidin channels are embedded;[45] such protein-induced membrane deformations incur an energy penalty[33] that depends on the composition of the membrane.

Another energy term potentially contributing to the hydrophobic mismatch effect is due to the "residual mismatch" that arises from the incomplete alleviation of the hydrophobic mismatch by the membrane deformation (**Figure 2**). Indeed, from lipid association electron paramagnetic resonance (EPR)

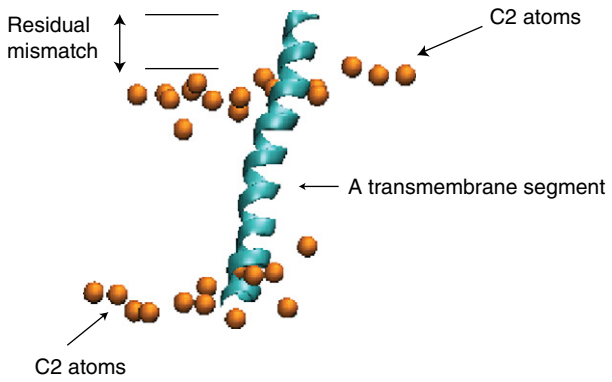

Figure 2 Schematic illustration of *membrane deformations* and *residual mismatch*. The figure is taken from a snapshot of MD simulations of rhodopsin in lipid bilayer, and shows a transmembrane segment whose hydrophobic thickness is greater than the basal thickness of the lipid bilayer. The hydrophobic mismatch leads to membrane deformations and the residual mismatch shown.

studies,[46] residual mismatch was inferred to be a major contributor to the hydrophobic mismatch cost for several multihelical transmembrane proteins.

9.12.3 Framework for Quantitative Description of Lipid-Protein Interactions

Having introduced several key aspects in membrane-protein interactions, viz., site-specific interactions between lipid and protein, membrane deformations and the associated membrane deformation energy, and the residual mismatch energy, we now turn to the computational framework that enables a quantitative description of all these critical interaction measures. The mechanistic insights provided by such quantification of the role of the lipid environment in the integral protein function are illustrated by the specific applications described in Section 9.12.4.

9.12.3.1 Description of Membrane Deformation

The shape of a deformed membrane around the inserted protein can be quantified by the deformation variable $u(x,y)$ defined locally per bilayer leaflet as:[33]

$$u(x,y) = \frac{1}{2}\left(d(x,y) - d_0\right) \quad [1]$$

where $d(x,y)$ and d_0 are the local and bulk bilayer thicknesses, respectively. These thicknesses are typically calculated either from the C2–C2 distances (which represent the hydrophobic thickness of the bilayer), or the phosphate-phosphate distances (which correspond to the peak-to-peak separation on the electron density profiles obtained from X-ray diffraction studies[47]).

The variable $u(x,y)$ can be obtained, for example, from regular atomic MD simulations during the production part of the MD trajectory, using eqn [1] and by measuring $d(x,y)$ through the positions of the phosphate/C2 atoms on the opposing leaflets fitted onto a grid. Usually, as in eqn [1], the analysis is simplified by taking $u(x,y)$ to be the average of the deformations in the two leaflets of the bilayer, as opposed to treating the two leaflets separately. This simplification is possible only if the volumes occupied by the protein in the two leaflets are approximately aligned one above another, and the local deformations are small and approximately similar in both leaflets. On the other hand, in systems involving different lipid compositions in the two leaflets, or highly tilted protein, the two leaflets should preferably be treated as separate monolayers.

The membrane shape can also be calculated from eqn [1] in the context of a more coarse-grained framework, such as continuum elastic formulation, whereby the lipid membrane is represented as continuum two-dimensional deformable media. Importantly, such coarse-graining allows quantification of the corresponding free energies, as we show next.

9.12.3.2 Energy Cost of Hydrophobic Mismatch

The free energy penalty due to the hydrophobic mismatch is the sum of the membrane elastic deformation energy ΔG_{def} and the residual mismatch energy ΔG_{res}:[46]

$$\Delta G_{\phi} = \Delta G_{def} + \Delta G_{res} \quad [2]$$

In the continuum formulation, the membrane is represented as a continuum elastic medium that can deform locally according to its elastic moduli K_c (for splay-distortion) and K_a (for compression-extension), α (the coefficient of surface tension), and the monolayer spontaneous curvature C_o. The macroscopic parameters K_c and K_a are experimentally available for several lipid membranes. If one of these parameters is not known for a given lipid membrane, it can be inferred using the well-known relation $K_c \propto K_a d_0^2$. C_0 is also available experimentally for many lipids. For mixtures of different lipids, C_0 can be obtained from the mole fractions μ_i and spontaneous curvatures C_i of the individual components, using the relationship:[48,49]

$$C_0 = \sum_i \mu_i C_i$$

ΔG_{def} in eqn [2] is determined by contributions from compression-extension, splay-distortion, and surface tension terms, and is given by:[33]

$$\Delta G_{def} = \frac{1}{2}\int_{\Omega}\left\{K_a\frac{(2u)^2}{{d_0}^2} + K_c\left(\frac{\partial^2 u}{\partial x^2} + \frac{\partial^2 u}{\partial y^2} - C_o\right)^2 + \alpha\left(\left(\frac{\partial u}{\partial x}\right)^2 + \left(\frac{\partial u}{\partial y}\right)^2\right)\right\} d\Omega \quad [3]$$

With these energy terms, the continuum theory has successfully explained the lifetimes of gramicidin channels in different lipid bilayers.[33,34]

In certain special cases, such as membrane compositions involving high levels of cholesterol and saturated lipids, the membrane deformation energy may need to be complemented by an additional energy cost corresponding to the lipid packing at the lipid/protein interface.[24] Equation [3] also neglects the Gaussian curvature term, which will be important for systems undergoing topological changes such as in the lipidic cubic phases, but can be safely neglected in the bilayer phase.

The residual mismatch energy penalty ΔG_{res} in eqn [2] arises from an incomplete alleviation of hydrophobic mismatch due to the high energy cost of membrane deformation, and penalizes unfavorable hydrophobic-hydrophilic interactions at the protein/lipid interface. ΔG_{res} can be approximated as being linearly proportional to the involved surface area at the protein-membrane interface,[50,51] and thus it is estimated as the sum of the residual energy penalties at each TM:

$$\Delta G_{res} = \sum_{i=1}^{N_{TM}} \Delta G_{res,i} \sim \sum_{i=1}^{N_{TM}} \sigma_{res} SA_{res,i} \quad [4]$$

where $SA_{res,i}$ is the surface area of the ith TM participating in the unfavorable hydrophobic-hydrophilic interactions, the constant of proportionality σ_{res} is available from literature to be $\sim$0.028 kcal/(mol A^2),[50,51] and N_{TM} is the number of TMs of the protein.

In the continuum formulation, the equilibrium membrane shape around the inserted protein corresponds to a minimum

in the value of the free energy ΔG_ϕ composed of the $\Delta G_{def} + \Delta G_{res}$ terms. Noting that ΔG_{res} arises from *interfacial* protein/lipid interactions, the steady-state $u(x,y)$ can be obtained by minimizing ΔG_{def} with respect to local bilayer deformations $u(x,y)$ subject to the appropriate boundary conditions on the protein/lipid interface. This can be accomplished using the Euler-Lagrange formulation, which leads to the following boundary value problem:[33]

$$K_C\nabla^4 u - \alpha\nabla^2 u + \frac{4K_a}{{d_0}^2}u = 0,$$
$$u|_{\Gamma_{in}} = u_0(x,y), \quad u|_{\Gamma_{out}} = 0, \quad \nabla^2 u|_{\Gamma_{in}} = v_0(x,y), \quad \nabla^2 u|_{\Gamma_{out}} = 0 \qquad [5]$$

where Γ_{in} and Γ_{out} denote the protein-membrane and the outer boundary. The boundary condition on the curvature could alternatively be on the slope. We should note that the lipid packing near the protein enters the formulation through the slope boundary condition.

9.12.3.3 Solving for Membrane Deformation

Because eqn [5] contains a *fourth order* partial differential equation, solving the corresponding boundary value problem even numerically is non-trivial. Therefore, we first discuss two common simplifying assumptions, and then provide the strategy to obtain $u(x,y)$ and ΔG_{def} without using any of these assumptions. The use of these assumptions greatly influences the scope and complexity of the method, and should be guided by careful consideration of the system of interest and the questions being asked of the model.

Assumption #1 – Assuming radial symmetry: For *single TM* proteins, the continuum calculations can usually be simplified by assuming radial symmetry of the protein structure and membrane deformations around the protein. With this assumption, the partial differential equation for $u(x,y)$ simplifies to an ordinary differential equation for $u(r)$ where r is the radial distance from the protein-membrane boundary, and each of the boundary conditions is a scalar value (see eqn [6]). This ordinary differential equation can be solved using standard numerical ODE solvers.

$$K_C\frac{d^4u}{dr^4} - \alpha\frac{d^2u}{dr^2} + \frac{4K_a}{{d_0}^2}u = 0,$$
$$u|_{\Gamma_{in}} = u_0, \quad u|_{\Gamma_{out}} = 0, \quad \frac{du}{dr}|_{\Gamma_{in}} = s_0, \quad \frac{du}{dr} = 0 \qquad [6]$$

Assumption #2 – Assuming strong hydrophobic coupling: For the boundary condition on u at the protein-membrane interface, several works in the literature have assumed that the membrane deformations completely alleviate the hydrophobic mismatch, an assumption referred to as strong hydrophobic coupling. The boundary condition u_0 can be obtained by comparing experimental estimates of the basal thickness of the lipid bilayer and the hydrophobic length of the protein. However, the residual mismatch may be an important aspect of the problem, in which case this assumption cannot be made. For example, the hydrophobic mismatch between the lipid bilayer and the protein may be too large to be alleviated by membrane deformations alone.

9.12.3.3.1 Solving the PDE without assumptions of radial symmetry and strong hydrophobic coupling

For multi-segment transmembrane proteins, the lengths of the hydrophobic stretches of different TM segments differ, e.g., TM1 of the 7-TM rhodopsin is longer than TM4 by 7–8 Ang. The pattern of hydrophobic thickness will likely result in an asymmetric membrane deformation profile around the protein incorporating such TM segments. Furthermore, from lipid association EPR studies, the residual mismatch has been inferred to be a substantial component of the energy cost for a number of multi-segment TM proteins,[46] and this residual mismatch may vary from TM to TM. Thus, for multi-helical TM proteins in particular, the method is more powerful if neither Assumption #1 or #2 is made while solving eqn [5].

To solve eqn [5] without Assumption #1 of radial symmetry requires boundary conditions for the entire membrane-protein boundary. At the same time, releasing Assumption #2 means that the boundary condition $u_0(x,y)$ at the protein-membrane interface cannot be taken to be the membrane deformation that allows the hydrophobic length of the deformed membrane to match that of the protein; that is, the information of $u_0(x,y)$ cannot be obtained simply by comparing the basal thickness of the membrane and the hydrophobic length of the protein. Therefore, we have developed a multi-scale strategy of augmenting the continuum calculations with specific inputs from cognate MD simulations.[52] Specifically, we obtain the following inputs from cognate MD:Γ_{in}, Γ_{out}, $u_0(x,y)$, and average membrane thickness d_0 at Γ_{out}. The boundary condition for membrane curvature at the protein/lipid interface $v_0(x,y)$ can be obtained from MD, or from a self-consistent approach using optimization. Notably, the multi-scale strategy does not invoke symmetry either in the membrane/protein boundary Γ_{in} or in the membrane deformations $u(x,y)$, but rather treats Γ_{in} as an irregular contour and allows for radially asymmetric changes in the membrane shape.

To follow this strategy in solving the boundary value problem in eqn [5] without introducing any simplifying assumption of radial symmetry, we converted the fourth order differential eqn [5] in $u(x,y)$ to a couple of simultaneous Poisson equations in membrane deformation u and membrane curvature v:[53–55]

$$K_c\nabla^2 v - \alpha v + \frac{4K_a}{{d_0}^2}u = 0,$$
$$\nabla^2 u = v,$$
$$u|_{\Gamma in} = u_0(x,y), \quad u|_{\Gamma out} = u_1(x,y), \quad v|_{\Gamma in} = v_0(x,y),$$
$$v|_{\Gamma out} = v_1(x,y) \qquad [7]$$

Equation [7] can be solved numerically for $u(x,y)$ on a rectangular grid using a standard finite difference scheme for Poisson equations. In the illustration of the approach presented in the next section, eqn [7] was discretized using the central 5-point approximation of the Laplacian operator,[56] and the system then solved using the iterative Gauss-Siedel algorithm, which typically takes 125–150 iterations to converge in our calculations.

To obtain the boundary condition $v_0(x,y)$ self-consistently, an optimization procedure can be used to search for $v_0(x,y)$ that would globally minimize ΔG_{def}. To reduce the complexity

of the optimization problem, $v_0(x,y)$ is first expressed as a truncated Fourier series,

$$v_0(x,y) : v_0(\theta) \sim \sum_{n=0}^{7} \{a_n \cos(n\theta) + b_n \sin(n\theta)\} \quad [8]$$

where θ is the polar angle corresponding to the coordinates (x,y), and a_n and b_n are the Fourier coefficients. Then, for any given $\{a_n, b_n\}$, eqn [7] gives the membrane deformation profile, and eqn [3] the corresponding ΔG_{def}. The non-linear optimization problem is solved with the objective function $\Delta G_{def} = f\{a_n, b_n\}$. In our practice, we use the BFGS optimization algorithm,[57] which is a standard global, quasi-Newtonian optimization procedure. Every optimization calculation should be performed in three or more replicates, each starting with a random seed.

9.12.3.4 Quantifying the Residual Mismatch Energy

Quantification of the residual mismatch energy using eqn [4] requires the determination of the surface area $SA_{res,i}$ involved in unfavorable hydrophobic-hydrophilic interactions between the lipids and the protein. This can be done by comparing the hydrophobic part of the TM to the hydrophobic part of the surrounding membrane.

One strategy to do this comparison in practice would be to use solvent accessible surface area (SASA) calculations in the following steps.

1. Calculate the membrane thickness $L_{mem,i}$ near the ith TM. For this, calculate the average membrane thickness within an angular sector spanning the TM and within a cut-off distance corresponding to about one lipid shell.
2. Let the hydrophobic thickness of the ith TM be denoted by L_i. Compare $L_{mem,i}$ and L_i.
   a. If $L_i > L_{mem,i}$, identify the hydrophobic residues of the TM located beyond the hydrophobic part of the membrane. Note that interfacial tryptophan can be assumed to not contribute to hydrophobic mismatch.
   b. If $L_i > L_{mem,i}$, indentify the hydrophilic residues sitting inside the membrane's hydrophobic core. Note that the interfacial lysine and arginine residues would usually not contribute to the residual mismatch due to the snorkeling effect. Also, serine and threonine residues are polar, but these residues may not contribute to the residual mismatch even if they are sitting within the hydrophobic part of the membrane, as their polar parts can form H-bonds with the helix backbone.
3. From the MD trajectory, calculate the SASA of each residue with the solute being the protein + hydrophobic part of the bilayer and just the protein respectively. The software NACCESS can be used to calculate the SASA values (http://www.bioinf.manchester.ac.uk/naccess/).
4. a. If $L_i > L_{mem,i}$, then $SA_{res,i} = \text{SASA}\ \{\text{solute} = \text{protein} + \text{hydrophobic part of the bilayer}\}$
   b. If $L_i < L_{mem,i}$, $SA = SASA\ \{\text{solute} = \text{protein}\} - SASA\ \{\text{solute} = \text{protein} + \text{hydrophobic part of the membrane}\}$
5. Use $SA_{res,i}$ values in eqn [4] to obtain the residual mismatch at each TM.

An alternative strategy would be to use the fact that the residual mismatch energy is proportional to $|L_{mem,i} - L_i|$ and to the perimeter at the lipid-protein interface.[46] However, we have found that in practice that it is difficult to obtain precise values for the perimeter at each individual TM.

9.12.3.5 Site-Specific Protein-Lipid Interactions

In addition to the residual mismatch, other site-specific protein-lipid interactions described in Section 9.12.2 play an important role in regulating protein function. These direct interaction modes between membrane components and proteins can be identified from long time-scale atomistic molecular dynamics simulations of the protein/membrane system. These interactions are specific to the system of interest, and have to be analyzed on a case-by-case basis. For example, if interaction with cholesterol is of interest, then atomistic simulation of the protein in a lipid mixture containing cholesterol would (1) show if cholesterol is more concentrated near the protein, and (2) allow the identification of specific residues in the protein molecule that interact preferentially with cholesterol. To be useful, such an analysis must be carried out on sufficiently long (preferably microsecond order) MD trajectories[41] or on several independent trajectories of the same system each starting with a random seed,[43] so that different lipid components can sample various regions around the insertion and establish stable direct interactions with the protein.

To summarize, in this section we have presented a quantitative framework that combines molecular dynamics with continuum elastic calculations to quantify the membrane deformations and the corresponding deformation energy along with residual mismatch at each TM. We call this approach 3D-CTMD, and illustrate it in the next section with applications to membrane-driven oligomerization and the role of cholesterol in the spatial organization of the membrane-partitioning GPCR ligands.

9.12.4 Illustrative Applications

We show below how the quantitative biophysical framework for the calculation of membrane remodeling presented in this chapter, based on a combination of continuum-level formulations with data from all atom MD simulations, can provide insightful information in systems containing both single-helical and multiple-TM proteins.

9.12.4.1 Application to Single Helical Proteins: Role of Cholesterol in the Spatial Organization of the Membrane-Partitioning GPCR Ligands

As mentioned in Section 9.12.1, the efficacy of several different GPCRs has been found to change in cholesterol-rich raft nanodomains. The cholesterol (Chol) rich environment of the membrane affects not only the receptors, but also certain GPCR ligands that are known to reach their binding sites after partitioning into the membrane. A specific example is that of the kappa-opioid receptor (KOR)[58] and its endogenous ligand DynorphinA (DynA).[14,15]

To investigate a possible effect of cholesterol on the organization of DynA-membrane system, we have performed all-atom, explicit-solvent 150 ns molecular dynamics simulations of (1)

DynA in a DMPC bilayer, and (2) DynA in a DMPC bilayer containing 20% cholesterol (three independent simulations for the cholesterol-containing case).[24] A comparison of the equilibrated parts of the two MD trajectories showed that DynA sits about 5 Å higher in the cholesterol-containing bilayer (Figure 3), and is also less tilted with respect to the membrane normal in the cholesterol-containing bilayer. These findings from the MD simulations are mechanistically suggestive when taken together with earlier reports on the interaction pathway of Dyn10,[59] a shorter analogue of DynA with a truncated C-terminus, as well as the cannabinoid ligand 2-AG.[12] These reports indicated that the entry pathway is close to the bilayer-water interface, so that the effect of cholesterol on the membrane positioning of DynA can be expected to aid the migration of DynA towards its binding site in the GPCR. The facilitated entry of the ligand in the cholesterol-containing

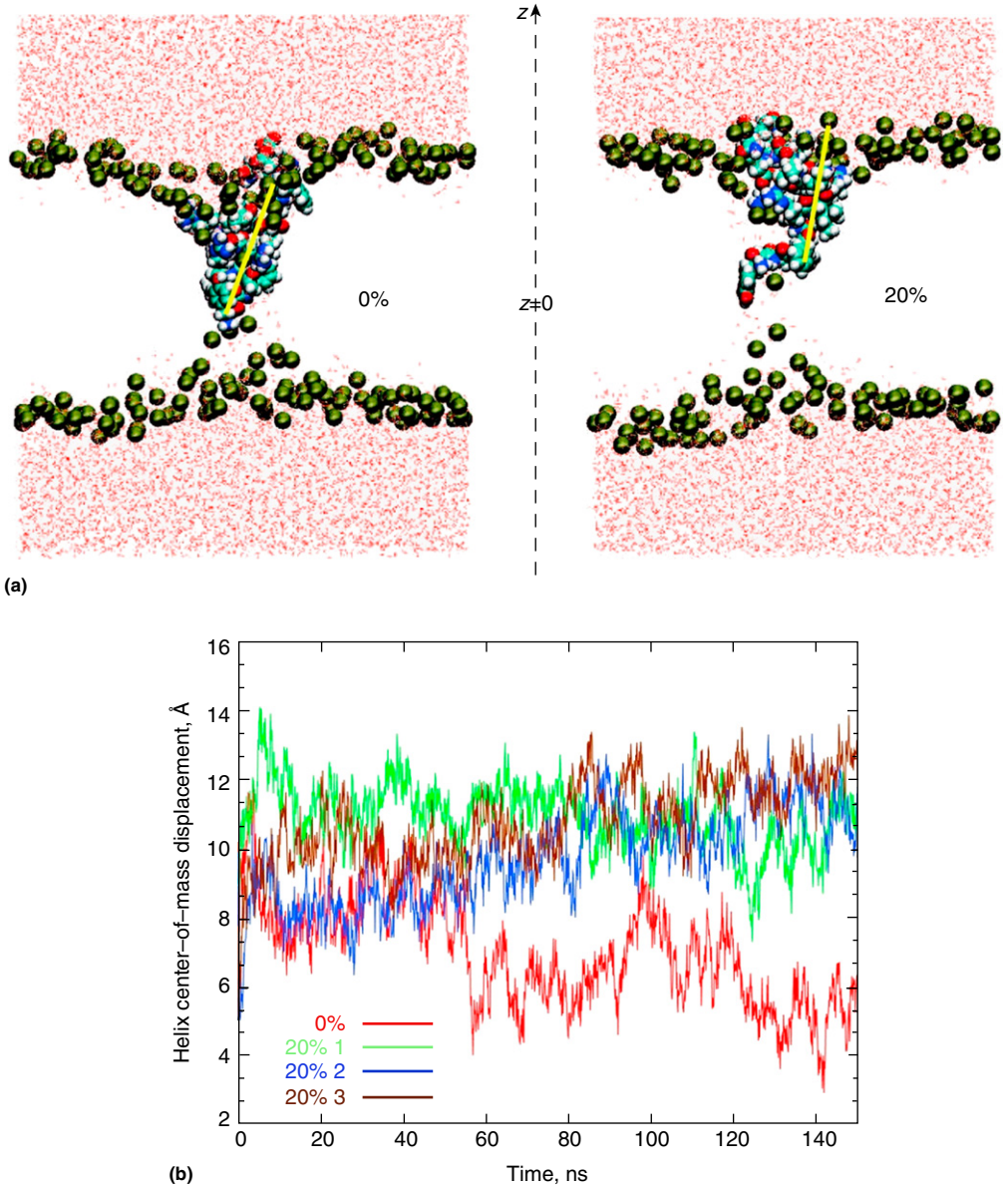

Figure 3 Molecular Dynamics Simulations of dynorphin *A* 1–17 (DynA) peptide in cholesterol-enriched lipid bilayers. (a) Final snapshots, after 150 ns, of DynA interacting with pure DMPC (left) and DMPC/Chol (right) membranes. DynA is in space-fill, and the membrane shape is depicted by the positions of phosphate atoms (colored in gold) on the two membrane leaflets. For clarity, the remaining DMPC and cholesterol atoms as well as the salt ions are removed. Waters surrounding membranes are shown in red. The bilayer normal *z* axis is drawn to highlight the location of the bilayer midplane ($z = 0$), and yellow lines are visual guides to illustrate different extents of DynA tilting in DMPC and DMPC/Chol membranes. (b) DynA dynamics in the model membranes DMPC and DMPC containing 20% cholesterol. Evolution of the vertical displacement from the bilayer midplane of the DynA 4–9 segment center of mass in the simulated systems is shown. Three independent trajectories for the DMPC/cholesterol system are represented by different traces. Reproduced with permission from Figures 4 and 5 in Khelashvili, G.; Mondal, S.; Andersen, O. S.; Weinstein, H. Cholesterol modulates the membrane effects and spatial organization of membrane-penetrating ligands for G-protein coupled receptors. *J. Phys. Chem. B* **2010**, *114*, 12046–12057. Copyright by American Chemical Society.

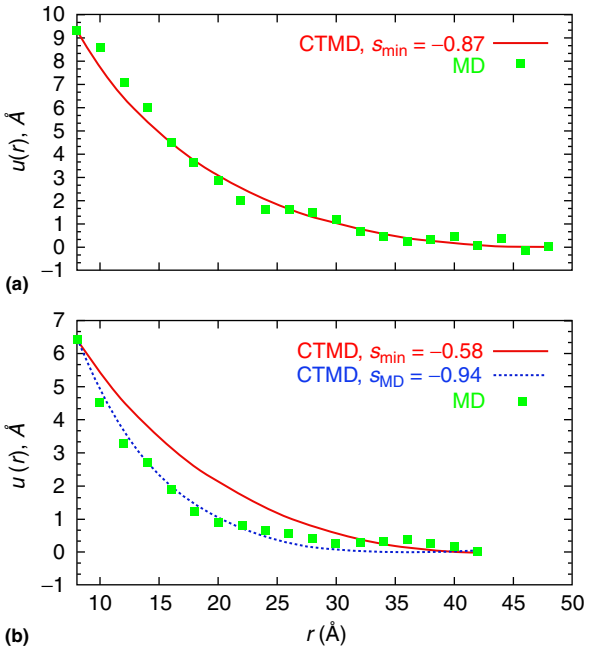

Figure 4 Comparison of DynA-induced membrane deformations obtained from MD simulations and from 3D-CTMD theory for DMPC (a) and DMPC/Chol (b) bilayers. Assumption #1 is applied: radial symmetry of protein shape and membrane deformations, so that profiles of membrane deformations $u(r)$ are shown as a function of radial distance r from DynA. For DMPC/Chol, the data are averaged over three independent trajectories described in ref. Khelashvili, G.; Mondal, S.; Andersen, O. S.; Weinstein, H. *J. Phys. Chem. B.* The MD predictions are depicted as symbols, and equilibrium shapes from the self-consistent 3D-CTMD are plotted as solid lines. The 3D-CTMD solutions in both panels correspond to the values of packing parameter s_{min} that minimize the free energy functional in eqn [6]. For the DMPC/Chol system. An alternative solution for $u(r)$ obtained from 3D-CTMD based on the value of the packing parameter obtained from the MD simulations is illustrated by the dashed line. For 3D-CTMD calculations, r_0 was set to 8 Å as the average radius of the DynA helix derived from the MD simulations, and elastic parameters were based on experimental results and are listed in Table 2 of ref below. Reproduced with permission from Figure 10 in Khelashvili, G.; Mondal, S.; Andersen, O. S.; Weinstein, H. Cholesterol modulates the membrane effects and spatial organization of membrane-penetrating ligands for G-protein coupled receptors. *J. Phys. Chem. B* **2010**, *114*, 12046–12057. Copyright by American Chemical Society.

bilayers may explain the higher efficacy of the Kappa Opioid Receptor (KOR) in such regions of the cell membrane.[58]

We applied the 3D-CTMD calculation framework described in this chapter to quantify the membrane deformations and the corresponding energy contributions to the behavior of DynA in the two types of bilayer discussed above. For this system we used simplifying Assumption #1 that is, radial symmetry (see Section 9.12.3) because the membrane immersed region of DynA is a single helical peptide. The membrane deformations u were therefore represented as a function of the radial distance r. **Figure 4** shows the $u(r)$ obtained directly from the MD simulations, compared to the results obtained from solving eqn [6] using the combined MD-continuum strategy. For the boundary conditions of eqn [6], we used u values from the MD simulations obtained at the dynorphin-membrane interface, and in the bulk. The boundary condition for the slope at the DynA-membrane interface was obtained from separate calculations in which the slope was either taken directly from MD (s_{MD}) or obtained from self-consistent calculations that minimize ΔG_{def} with respect to s.

Comparing $u(r)$ taken directly from MD to results from 3D-CTMD illustrates an important point about the method: the MD and the continuum calculations give similar results for $u(r)$ if s is obtained directly from MD. On the other hand, for the calculation in which the s_{min} was obtained by minimizing the energy functional in eqn [2] (Section 9.12.3), the two solutions match for the DMPC bilayer, but not for the cholesterol-containing bilayer. This can be explained by the fact that the continuum energy function does not contain a term for the lipid tail packing energy at the membrane-protein interface, and treats the lipid packing implicitly through the boundary condition on s_{min}.[45] Therefore, if this missing energy term becomes important, as it does in lipid mixtures of saturated bilayers and cholesterol, the s_{min} will be inaccurate.

In addition to providing the shape of the membrane $u(r)$ in the two cases, the method also allows comparison of the deformation free energies: 6.84 kT for pure DMPC and a much larger value of 36.8 kT for the cholesterol-containing DMPC bilayer (calculated with $s = s_{MD}$).

9.12.4.2 Application to Multi-Segment Proteins: Membrane-Driven GPCR Oligomerization

The combined MD + continuum strategy can provide the same level of quantitative insight for membrane systems with embedded multi-helical transmembrane proteins.[52] This is illustrated here with calculations for the 7-transmembrane segment proteins rhodopsin (Rho) and the serotonin receptor subtype 2A (5-HT_{2A}R); two examples of G protein coupled receptors (GPCRs) that are prototypical for a system with crystallographically known structure (Rho), and a homology model using such structures as templates (5-HT_{2A}R). The Rho protein is immersed in a bilayer composed of the short-tailed $(C14:1)_2$PC lipid; the 5-HT_{2A}R structure is the result of simulation with bound ligand, the endogenous agonist serotonin (5-HT) and is immersed in a bilayer composed of the 7:7:6 1-stearoyl-2-docosahexaenoyl-*sn*-glycero-3-phosphocholine (SDPC)/1-palmitoyl-2-oleoyl-*sn*-glycero-3-phosphocholine (POPC)/cholesterol (Chol) lipid mixture. As shown below, the results of these calculations illustrate the ability of the novel method to quantify the membrane remodeling effects of multi-helical proteins and to yield mechanistic insights into the membrane-driven GPCR oligomerization discussed in Section 9.12.1 above.

9.12.4.2.1 Membrane remodeling by rhodopsin

The membrane remodeling profile was obtained from the MD trajectory by fitting a grid to the phosphate atoms during the production run, as described in Section 9.12.3. The steady state membrane shape was calculated self-consistently by using the continuum calculations (3D-CTMD) without any assumption of radial symmetry and strong hydrophobic coupling; that is, eqn [5], Section 9.12.3 (see **Figure 5(a)**). Although the 3D-CTMD framework assumes the membrane to be an elastic continuum, the deformed membrane shapes calculated here

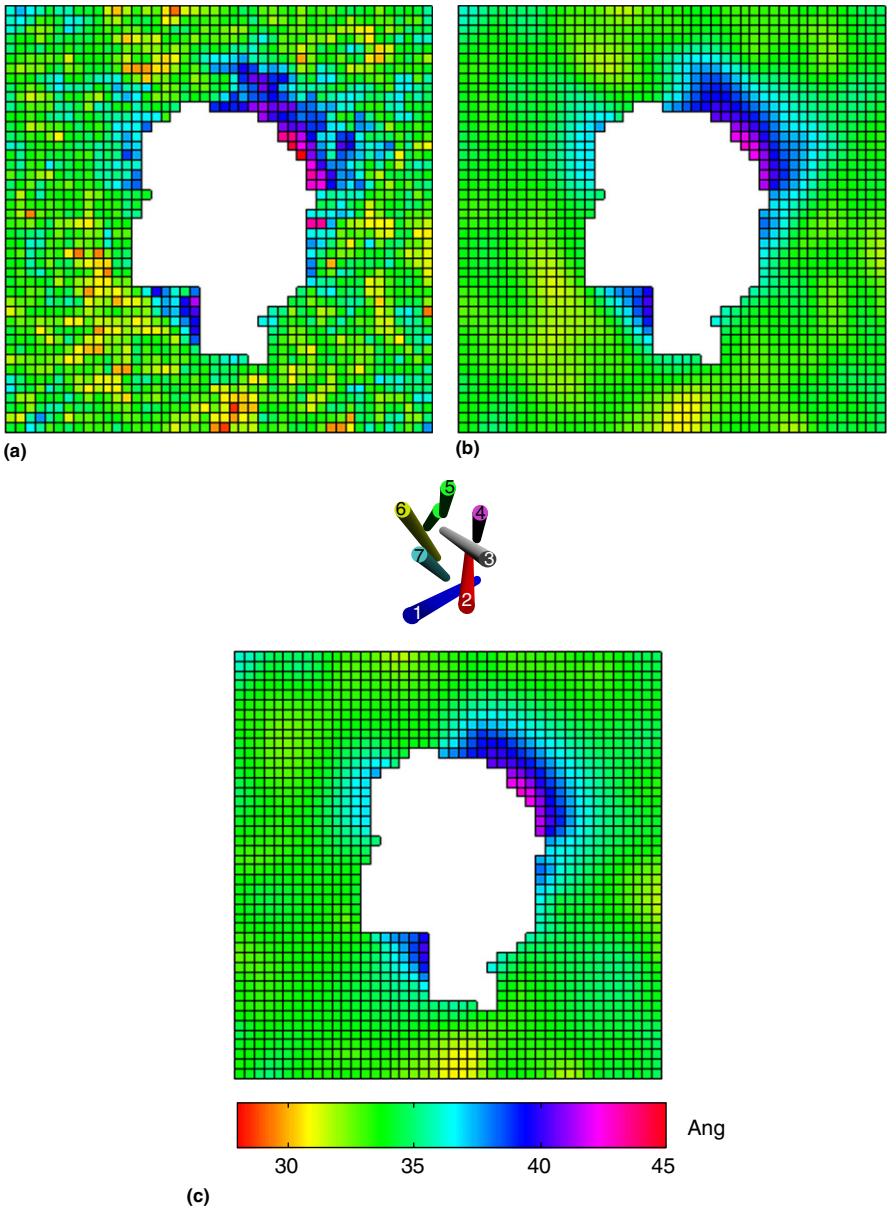

Figure 5 Application of the three-dimensional combined continuum and MD approach (3D-CTMD) to rhodopsin GPCR in $(C14:1)_2PC$ lipid bilayer. (a) Profile of membrane deformations around rhodopsin represented as time-averaged bilayer thickness from the MD trajectory mapped onto a rectangular grid. Each grid square is 2 Å by 2 Å. (b) Bilayer thickness profile after smoothing the deformation map in **Figure 5(a)**. (c) Steady-state membrane thickness profile obtained self-consistently from the continuum 3D-CTMD calculations and with thickness boundary condition at the protein-membrane interface and the outer boundary taken from the MD shape in **Figure 5(b)**. Note the close agreement between the profiles in **Figure 5(b)** and **(c)** (within 0.5 Å RMSD of each other). The scale indicates membrane thickness. The schematic cartoon of rhodopsin indicates the orientation of the molecule relative to the membrane.

with the new method are in excellent agreement with the smoothed membrane shape obtained directly from cognate MD simulations. This finding is consistent with the finding for the dynorphin-DMPC system discussed above, and with previously used assumptions[60] that molecular approaches and continuum elastic approaches would yield similar results at length scales comparable to the membrane thickness.

As the hydrophobic thickness of the $(C14:1)_2PC$ bilayer is shorter than that of the inserted Rho molecule, the tendency towards hydrophobic matching is expected to result in an average increase in the thickness of the membrane. We find that this is indeed the case, with the *average bilayer thickness* within 12 Å of the protein being about $\sim$2 Å larger than that in the bulk. This result, showing the average thickness increase near the protein to be rather small, is in good qualitative agreement with the results obtained from the solid state NMR experiments on rhodopsin in different PC membranes.[61] However, in addition to the average results obtainable from the NMR experiment, the 3D-CTMD method can quantify local membrane remodeling. Thus, the calculations identify substantial local thickening and

Table 1 Comparison of membrane thickness near each TM and the hydrophobic length of the TM for rhodopsin in $(C14:1)_2PC$[a]

TM	L_{mem} *(Å)*	L_{TM} *(Å)*	A_{res} *(Å²)*	ΔG_{res} *(k_BT)*
1	28.83	36.96	210	9.94
2	29.38	35.79	74	3.51
4	31.49	28.97	0	0
5	29.75	31.03	115	5.43
6	28.82	34.70	36	1.69
7	28.97	36.92	119	5.61

[a]Using the following TM definitions (given in the Ballesteros-Weinstein generic numbering[64,65]): 1.29–1.59 (TM1), 2.38–2.66 (TM2), 4.43–4.62 (TM4), 5.38–5.63 (TM5), 6.33–6.59 (TM6), 7.32–7.56 (TM7). The A_{res} values were calculated with the SASA-based recipe in of section C.4. with a probe radius of 1.4 Å. Probes with smaller radii did not change significantly the A_{res} estimates.

thinning of membranes around the different transmembrane (TM) segments of the protein. For example, a significant thickening of the $(C14:1)_2PC$ bilayer by $\sim$5 Å is observed around TM4. The membrane deformation free energy ΔG_{def} for the entire system is evaluated to be $\sim 4.7 k_BT$.

The residual mismatch for the multi-helical protein was calculated using eqn [4] and the algorithm presented in section 9.12.3.4. The details of the comparison of the TM hydrophobic length to the local bilayer thickness are presented in **Table 1**, together with the calculated residual SAs (A_{res}) and the mismatch energies ΔG_{res} at individual TMs. The results show that:

1. Although ΔG_{def} is substantial, ΔG_{res} is the dominant contribution to the overall ΔG_{ϕ} for this GPCR/membrane system, in agreement with inferences from lipid association studies of several multi-helical transmembrane proteins;[46] and
2. ΔG_{res} varies substantially among TMs.

These quantitative findings have direct implications for the types of effects on the functional properties of the proteins discussed in section 9.12.1.

9.12.4.2.1.1 Insights into membrane-driven rhodopsin oligomerization

A large hydrophobic mismatch energy experienced by the *monomeric* proteins in the lipid membrane can constitute a strong drive for association based on reduction of the total free energy of the membrane-embedded system. Thus, such an association can be expected to at least partially relieve the hydrophobic mismatch experienced by the monomer, by burying in the interface those parts of the protein that cause the largest contribution to the unfavorable ΔG_{res}. Consequently, the drive for oligomerization would be stronger at the TMs with the larger contribution to the mismatch. The variation in ΔG_{res} from TM to TM observed for the multi-helical proteins suggests that the stronger drive to oligomerize at certain TMs than at others may be an important determinant of the interfaces in such oligomerizations. With the results for rhodopsin in $(C14:1)_2PC$ as an example, this reasoning suggests maximal oligomerization drive at TM1. Combined with the large total energy penalty ΔG_{ϕ} (eqn [2]) for rhodopsin in $(C14:1)_2PC$, $\sim$31 k_BT, these results predict a large drive for rhodopsin oligomerization in $(C14:1)_2PC$, in agreement with the FRET studies and with inferences from previous calculations.[29]

9.12.4.2.2 Insights into membrane-driven serotonin 5-HT$_{2A}$R oligomerization

The illustration of the method by calculations on the serotonin receptor 5-HT_{2A}R in complex with the endogenous agonist 5-HT involve a more complex membrane system, which is composed of the lipid mixture 7:7:6 1-stearoyl-2-docosahexaenoyl-*sn*-glycero-3-phosphocholine (SDPC)/1-palmitoyl-2-oleoyl-*sn*-glycero-3-phosphocholine (POPC)/cholesterol (Chol). The choice of this lipid mixture brings the calculations closer to membrane compositions seen in biological systems, as the cell membranes in neural systems are usually rich in cholesterol and the highly unsaturated SDPC lipid,[62] while POPC is a common lipid in these membranes.

For this 3D-CTMD calculation, the 350 ns long all atom MD trajectory for 5-HT_{2A}R in complex with 5-HT and immersed in 7:7:6 SDPC/POPC/cholesterol lipid mixture contained molecular details about the conformational changes in response to the binding of 5-HT.[63] The results from the corresponding 3D-CTMD calculations revealed a distinct pattern of membrane deformations around the protein, with the largest extent of membrane thinning observed around TM6 (**Figure 6**), and substantial bilayer deformation around TM4 as well. **Table 2** lists the values of the residual mismatch for the constituent TMs which, like in the rhodopsin system

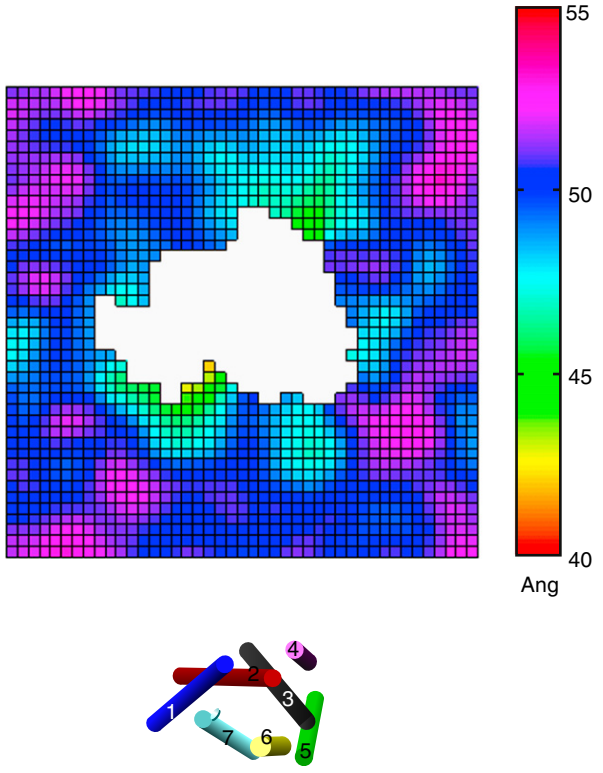

Figure 6 Steady state shape of 7:7:6 SDPC/POPC/cholesterol membrane surrounding the serotonin 5-HT_{2A} receptor complexed with the full agonist 5-HT. The scale indicates membrane thickness. The schematic cartoon of the serotonin $5HT_{2A}$ receptor indicates the orientation of the molecule relative to the membrane.

Table 2 Residual surfaces areas A_{res} (in Å^2) and corresponding residual energies ΔG_{res} (in k_BT) calculated for TMs of 5-HT_{2A}R in complex with 5-HT and immersed in the SDPC/POPC/cholesterol lipid bilayer

TM	A_{res} *(Å^2)*	ΔG_{res} *(k_BT)*
1	0	0
2	30	1.41
4	25	1.16
5	94	4.42
6	40	1.9
7	1	0

discussed previously, were substantial and TM-specific. The largest free energy penalty from the residual mismatch ($\sim 5\, k_BT$) is calculated at TM5, making this region the most likely to be involved in the interface of membrane-driven oligomerization of the 5HT-bound 5-HT_{2A}R. Notably, a recent report[63] shows that ligands with different measurable effects trigger differential structural perturbations, both in the GPCR and the surrounding membrane. These produce different extents of hydrophobic mismatch around the transmembrane (TM) helices. Thus, the mechanistic implications from the type of results presented here suggest that the interaction interfaces in the oligomers of the 5-HT_{2A}R will likely be different for the different ligands due to differences in the resulting hydrophobic mismatch between the receptor and the membrane. Allowing for radial asymmetry and residual mismatch, the 3D-CTMD formalism presented here has therefore offered a novel type of quantitative link between the perturbations of the GPCR structure produced by the binding of ligand, 5-HT, and the receptor oligomerization process. Notably, although the oligomerization process must reflect the combined properties and effects of all the participating protomers, the nature of the mismatch-alleviation effect suggests that the type of results illustrated here for the monomers provides the most essential information about the drive and likely interfaces.

9.12.5 Concluding Remarks

The quantitative biophysical framework for the calculation of membrane remodeling presented in this chapter is based on a combination of continuum-level formulations with data from all atom MD simulations. Combining the simulation results with the continuum elastic calculations can account for (1) radially asymmetric membrane deformations around the protein, and (2) residual mismatch. Given the evidence for the essential role played by the lipid environment in the function of membrane proteins (see Section 9.12.1), this level of quantitative information furthers our understanding of the biophysical basis for biomolecular function in the cell.

Using illustrative applications on both single-helical and multi-segment proteins, the 3D-CTMD approach presented here was applied to demonstrate how quantitative calculations of the membrane remodeling around protein can enrich our understanding of membrane protein function. We expect the new tools, enabling quantitative calculations for multi-helical transmembrane proteins, to serve well in furthering both theoretical and experimental biophysical considerations of the role of the lipid membrane in the many such systems of interest to cell and molecular physiology. As an example, if a GPCR has been observed to undergo a shift in the oligomerization interface due to pharmacologically different ligands, the illustrative calculations in Section 9.12.4 can be extended to investigate the role of the lipid environment in the ligand-induced shifts in the oligomerization interface.

Acknowledgments

We gratefully acknowledge the invaluable contribution of Olaf S. Andersen throughout the conceptual and practical development of the method. Support from National Institute of Health grants DA012408, DA012923, and U54 GM087519 and the computational resources of

1. The David A. Cofrin Center for Biomedical Information in the HRH Prince Alwaleed Bin Talal Bin Abdulaziz Alsaud Institute for Computational Biomedicine at Weill Medical College of Cornell University,
2. The New York Blue Computational Science facility housed at Brookhaven national lab, and
3. The Teragrid supercomputer allocation MCB090132, are greatly acknowledged.

We also thank other members of the Weinstein lab, in particular Jufang Shan and Niklaus Johner, for helpful discussions.

References

[1] Engelman, D. M. Membranes are more mosaic than fluid. *Nature* **2005**, *438*, 578–580.
[2] Phillips, R.; Ursell, T.; Wiggins, P.; Sens, P. Emerging roles for lipids in shaping membrane-protein function. *Nature* **2009**, *459*, 379–385.
[3] Soubias, O.; Teague Jr. W. E.; Hines K. G.; Mitchell D. C.; Gawrisch K. Contribution of Membrane Elastic Energy to Rhodopsin Function. *Biophys. J.* **2010**, *99*, 817–824.
[4] Soubias, O.; Teague, W. E.; Gawrisch, K. Evidence for specificity in lipid-rhodopsin interactions. *J. Biol. Chem.* **2006**, *281*, 33233.
[5] Lundbaek, J. A.; Birn, P.; Tape, S. E.; Toombes, G. E. S.; Søgaard, R.; Koeppe, R. E.; Gruner, S. M.; Hansen, A. J.; Andersen, O. S. Capsaicin regulates voltage-dependent sodium channels by altering lipid bilayer elasticity. *Mol. Pharmacol.* **2005**, *68*, 680.
[6] Brown, M. F.; Thurmond, R. L.; Dodd, S. W.; Otten, D.; Beyer, K. Elastic deformation of membrane bilayers probed by deuterium NMR relaxation. *J. Am. Chem. Soc* **2002**, *124*, 8471–8484.
[7] Marsh, D. Protein modulation of lipids, and vice-versa, in membranes. *Biochim. Biophys. Acta (BBA)-Biomembranes* **2008**, *1778*, 1545–1575.
[8] Lundbaek, J. A.; Collingwood, S. A.; Ingólfsson, H. I.; Kapoor, R.; Andersen. O. S. Lipid bilayer regulation of membrane protein function: gramicidin channels as molecular force probes. *J. R. Soc. Interface* **2010**, *7*, 373.
[9] Ostrom, R. S.; Insel, P. A. The evolving role of lipid rafts and caveolae in G protein coupled receptor signaling: implications for molecular pharmacology. *Br. J. Pharmacol.* **2004**, *143*, 235–245.
[10] Chini, B.; Parenti, M. G-protein coupled receptors in lipid rafts and caveolae: how, when and why do they go there? *J. Mol. Endocrin.* **2004**, *32*, 325.
[11] Bari, M.; Battista, N.; Fezza, F.; Finazzi-Agrò, A.; Maccarrone, M. Lipid rafts control signaling of type-1 cannabinoid receptors in neuronal cells. *J. Biol. Chem.* **2005**, *280*, 12212.
[12] Hurst, D. P.; Grossfield, A.; Lynch, D. L.; Feller, S.; Romo, T. D.; Gawrisch, K.; Pitman, M. C.; Reggio. P. H. A lipid pathway for ligand binding is necessary for a cannabinoid G protein-coupled receptor. *J. Biol. Chem.* **2010**, *285*, 17954.

[13] Pei, Y.; Mercier, R. W.; Anday, J. K.; Thakur, G. A.; Zvonok, A. M.; Hurst, D.; Reggio, P. H.; Janero, D. R.; Makriyannis, A. Ligand-binding architecture of human CB2 cannabinoid receptor: evidence for receptor subtype-specific binding motif and modeling GPCR activation. *Chem. Biol.* **2008**, *15*, 1207–1219.

[14] Schwyzer, R. Peptide-membrane interactions and a new principle in quantitative structure-activity relationships. *Biopolymers* **1991**, *31*, 785–792.

[15] Schwyzer, R. 100 Years lock and key concept: Are peptide keys shaped and guided to their receptors by the target cell membrane? *Biopolymers* **1995**, *37*, 5–16.

[16] Wiedmann, T. S.; Pates, R. D.; Beach, J. M.; Salmon, A.; Brown., M. F. Lipid-protein interactions mediate the photochemical function of rhodopsin. *Biochemistry* **1988**, *27*, 6469–6474.

[17] Gibson, N. J.; Brown, M. F. Lipid headgroup and acyl chain composition modulate the MI–MII equilibrium of rhodopsin in recombinant membranes. *Biochemistry* **1993**, *32*, 2438–2454.

[18] Brown, M. F. Modulation of rhodopsin function by properties of the membrane bilayer. *Chem. Phys. Lipids* **1994**, *73*, 159–180.

[19] Huber, T.; Botelho, A. V.; Beyer, K.; Brown, M. F. Membrane model for the G-protein-coupled receptor rhodopsin: hydrophobic interface and dynamical structure. *Biophys. J.* **2004**, *86*, 2078–2100.

[20] Botelho, A. V.; Gibson, N. J.; Thurmond, R. L.; Wang, Y.; Brown, M. F. Conformational energetics of rhodopsin modulated by nonlamellar-forming lipids. *Biochemistry* **2002**, *41*, 6354–6368.

[21] Gibson, N. J.; Brown, M. F. Role of phosphatidylserine in the MI-MIII equilibrium of rhodopsin. *Biochem. Biophys. Res. Commun.* **1991**, *176*, 915–921.

[22] Eroglu, Ç.; Brügger, B.; Wieland, F.; Sinning, I. Glutamate-binding affinity of Drosophila metabotropic glutamate receptor is modulated by association with lipid rafts. *Proc. Nat. Acad. Sci. USA* **2003**, *100*, 10219.

[23] Whorton, M. R.; Jastrzebska, B.; Park, P. S. H.; Fotiadis, D.; Engel, A.; Palczewski, K.; Sunahara, R. K. Efficient coupling of transducin to monomeric rhodopsin in a phospholipid bilayer. *J. Biol. Chem.* **2008**, *283*, 4387.

[24] Khelashvili, G.; Mondal, S.; Andersen, O.S.; Weinstein, H. Cholesterol modulates the membrane effects and spatial organization of membrane-penetrating ligands for G-protein coupled receptors. *J. Phys. Chem. B* **2010**, *114*, 12046–12057.

[25] Panetta, R.; Greenwood, M. T. Physiological relevance of GPCR oligomerization and its impact on drug discovery. *Drug Discov. Today* **2008**, *13*, 1059–1066.

[26] Terrillon, S.; Bouvier, M. Roles of G-protein-coupled receptor dimerization. *EMBO Rep.* **2004**, *5*, 30–34.

[27] Han, Y.; Moreira, I. S.; Urizar, E.; Weinstein, H.; Javitch, J. A. Allosteric communication between protomers of dopamine class A GPCR dimers modulates activation. *Nature Chem. Biol.* **2009**, *5*, 688–695.

[28] Botelho, A. V.; Huber, T.; Sakmar, T. P.; Brown, M. F. Curvature and hydrophobic forces drive oligomerization and modulate activity of rhodopsin in membranes. *Biophys. J.* **2006**, *91*, 4464–4477.

[29] Periole, X.; Huber, T.; Marrink, S. J.; Sakmar, T. P. G protein-coupled receptors self-assemble in dynamics simulations of model bilayers. *J. Am. Chem. Soc.* **2007**, *129*, 10126–10132.

[30] Mancia, F.; Assur, Z.; Herman, A. G.; Siegel, R.; Hendrickson, W. A. Ligand sensitivity in dimeric associations of the serotonin 5HT2c receptor. *EMBO Rep.* **2008**, *9*, 363–369.

[31] Fung, J. J.; Deupi, X.; Pardo, L.; Yao, X. J.; Velez-Ruiz, G. A.; DeVree, B. T.; Sunahara, R. K.; Kobilka, B. K. Ligand-regulated oligomerization of 2-adrenoceptors in a model lipid bilayer. *EMBO J.* **2009**, *28*, 3315–3328.

[32] Guo, W.; Shi, L.; Filizola, M.; Weinstein, H.; Javitch, J. A. Crosstalk in G protein-coupled receptors: changes at the transmembrane homodimer interface determine activation. *Proc. Nat. Acad. Sci. USA* **2005**, *102*, 17495.

[33] Nielsen, C.; Goulian, M.; Andersen, O. S. Energetics of inclusion-induced bilayer deformations. *Biophys. J.* **1998**, *74*, 1966–1983.

[34] Huang, H. W. Deformation free energy of bilayer membrane and its effect on gramicidin channel lifetime. *Biophys. J* **1986**, *50*, 1061–1070.

[35] Lundbæk, J.A.; Koeppe, R.E.; Andersen, O.S. Amphiphile regulation of ion channel function by changes in the bilayer spring constant. *Proc. Nat. Acad. Sci. USA* **2010**, *107*, 15427.

[36] Bruno, M. J.; Koeppe, R. E.; Andersen, O. S. Docosahexaenoic acid alters bilayer elastic properties. *Proc. Nat. Acad. Sci. USA* **2007**, *104*, 9638.

[37] Hwang, T. C.; Koeppe, II R. E.; Andersen, O. S. Genistein can modulate channel function by a phosphorylation-independent mechanism: importance of hydrophobic mismatch and bilayer mechanics. *Biochemistry* **2003**, *42*, 13646–13658.

[38] Ingolfsson, H. I.; Koeppe, II R. E.; Andersen, O. S. Curcumin is a modulator of bilayer material properties. *Biochemistry* **2007**, *46*, 10384–10391.

[39] Hanson, M. A.; Cherezov, V.; Griffith, M. T.; Roth, C. B.; Jaakola, V. P.; Chien, E. Y. T.; Velasquez, J.; Kuhn, P.; Stevens, R. C. A specific cholesterol binding site is established by the 2.8 Ã… Structure of the human Î²-adrenergic receptor. *Structure* **2008**, *16*, 897–905.

[40] Cherezov, V.; Rosenbaum, D. M.; Hanson, M. A.; Rasmussen, S. G. F.; Foon, S. T.; Kobilka, T. S.; Choi, H. J.; Kuhn, P.; Weis, W. I.; Kobilka, B. K.; Stevens, R. C. High-resolution crystal structure of an engineered human Î²-adrenergic G protein-coupled receptor. *Science* **2007**, *318*, 1258–1265.

[41] Ruprecht, J. J.; Mielke, T.; Vogel, R.; Villa, C.; Schertler, G. F. X. Electron crystallography reveals the structure of metarhodopsin. *I. EMBO J.* **2004**, *23*, 3609–3620.

[42] Khelashvili, G.; Grossfield, A.; Feller, S. E.; Pitman, M. C.; Weinstein, H. Structural and dynamic effects of cholesterol at preferred sites of interaction with rhodopsin identified from microsecond length molecular dynamics simulations. *Proteins: Structure, Function, and Bioinformatics* **2009**, *76*, 403–417.

[43] Pitman, M. C.; Grossfield, A.; Suits, F.; Feller, S. E. Role of cholesterol and polyunsaturated chains in lipid-protein interactions: molecular dynamics simulation of rhodopsin in a realistic membrane environment. *J. Am. Chem. Soc.* **2005**, *127*, 4576–4577.

[44] Grossfield, A.; Feller, S. E.; Pitman, M. C. A role for direct interactions in the modulation of rhodopsin by -3 polyunsaturated lipids. *Proc. Nat. Acad. Sci. USA* **2006**, *103*, 4888.

[45] Harroun, T. A.; Heller, W. T.; Weiss, T. M.; Yang, L.; Huang, H. W. Experimental evidence for hydrophobic matching and membrane-mediated interactions in lipid bilayers containing gramicidin. *Biophys. J.* **1999**, *76*, 937–945.

[46] Marsh, D. Energetics of hydrophobic matching in lipid-protein interactions. *Biophys. J.* **2008**, *94*, 3996–4013.

[47] Pan, J.; Mills, T. T.; Tristram-Nagle, S.; Nagle, J. F. Cholesterol perturbs lipid bilayers nonuniversally. *Phys. Rev. Lett.* **2008**, *100*, 198103.

[48] Chen, Z.; Rand, R. P. The influence of cholesterol on phospholipid membrane curvature and bending elasticity. *Biophys. J.* **1997**, *73*, 267–276.

[49] Khelashvili, G.; Harries, D.; Weinstein, H. Modeling membrane deformations and lipid demixing upon protein-membrane interaction: the BAR dimer adsorption. *Biophys. J.* **2009**, *97*, 1626–1635.

[50] Choe, S.; Hecht, K. A.; Grabe, M. A continuum method for determining membrane protein insertion energies and the problem of charged residues. *J. Gen. Physiol.* **2008**, *131*, 563.

[51] Ben-Tal, N.; Ben-Shaul, A.; Nicholls, A.; Honig, B. Free-energy determinants of alpha-helix insertion into lipid bilayers. *Biophys. J.* **1996**, *70*, 1803–1812.

[52] Mondal, S.; Khelashvili, G.; Shan, J.; Anderson, O. S.; Weinstein, H. Quantitative modeling of membrane deformations by multihelical membrane proteins: application to G-protein coupled receptors. *Biophys. J.* **2011**, *101*, 2092–2101.

[53] Chen, G.; Li, Z.; Lin, P. A fast finite difference method for biharmonic equations on irregular domains and its application to an incompressible Stokes flow. *Adv. Comp. Math.* **2008**, *29*, 113–133.

[54] Ehrlich, L. W. Solving the biharmonic equation as coupled finite difference equations. *SIAM J. Num. Anal.* **1971**, *8*, 278–287.

[55] Smith, J. The coupled equation approach to the numerical solution of the biharmonic equation by finite differences. *I. SIAM J. Num. Anal.* **1968**, *5*, 323–339.

[56] Panaretos, A. H.; Aberle, J. T.; Díaz., R. E. The effect of the 2-D Laplacian operator approximation on the performance of finite-difference time-domain schemes for Maxwell's equations. *J. Comp. Phys.* **2007**, *227*, 513–536.

[57] Shanno, D. F. Conditioning of quasi-Newton methods for function minimization. *Math. Comput.* **1970**, *24*, 647–656.

[58] Xu, W.; Yoon, S. I.; Huang, P.; Wang, Y.; Chen, C.; Chong, P. L. G.; Liu-Chen, L. Y. Localization of the opioid receptor in lipid rafts. *J. Pharmacol. Exp. Ther.* **2006**, *317*, 1295.

[59] Paterlini, G.; Portoghese, P. S.; Ferguson, D. M. Molecular simulation of dynorphin A-(1–10) binding to extracellular loop 2 of the -opioid receptor. A model for receptor activation. *J. Med. Chem.* **1997**, *40*, 3254–3262.

[60] Goetz, R.; Gompper, G.; Lipowsky, R. Mobility and elasticity of self-assembled membranes. *Phys. Rev. Lett.* **1999**, *82*, 221–224.

[61] Soubias, O.; Niu, S. L.; Mitchell, D. C.; Gawrisch, K. Lipid- rhodopsin hydrophobic mismatch alters rhodopsin helical content. *J. Am. Chem. Soc.* **2008**, *130*, 12465–12471.
[62] Saiz, L.; Klein, M. L. Influence of highly polyunsaturated lipid acyl chains of biomembranes on the NMR order parameters. *J. Am. Chem. Soc.* **2001**, *123*, 7381–7387.
[63] Shan, J.; Khelashvili, G.; Mondal, S.; Weinstein H. Pharmacologically Distinct Ligands Induce Different States of 5-HT2AR and Trigger Different Membrane Remodeling: Implications For GPCR Oligomerization. *Biophys. J.* **2011**, *100*, 254.
[64] Ballesteros, J. A.; Weinstein, H. Integrated methods for the construction of three-dimensional models and computational probing of structure-function relations in G protein-coupled receptors. *Methods Neurosci.* **1995**, *25*, 366–428.
[65] Ballesteros, J. A.; Weinstein, H.; Stuart C. S. Integrated methods for the construction of three-dimensional models and computational probing of structure-function relations in G protein-coupled receptors. In Methods in Neurosciences. Academic Press, 1995, pp. 366–428.